ISSN: 0067-2904

Structural, Antibiofilm and Anticancer Properties of Mn_3O_4 Nanoparticles Synthesized Using Spinach Extract

Noor Mohammed Jasam, Lekaa K. Abdul Karem *

Departments of Chemistry, College of Education for Pure Sciences, Ibn Al-Haitham, University of Baghdad, Iraq

Received: 6/3/2025 Accepted: 20/7/2025 Published: 30/ 7/2026

Abstract

This study investigates an economical and environmentally friendly method for synthesizing Mn_3O_4 nanoparticles using spinach extract and manganese sulfate in an alkaline environment. The resulting Mn_3O_4 nanoparticles were characterized using different techniques such as FTIR, UV-visible, Scanning Electron Microscopy (SEM), X-ray diffraction (XRD), Energy-dispersive X-ray (EDX) and Zeta potential. The size of the average crystal was calculated to be 46.16 nm using Debye-Scherrer's equation, and the particle size was 18.7 nm in SEM some deformation was observed due to aggregation. Kinetic stability gave a stable value of -52.5 mV in the Zeta potential of Mn_3O_4Nps. The antibacterial effects of (25, 50 and 100) µg /ml concentrations of Mn_3O_4NPs against *Staphylococcus aureus, E.coil, and Candida fungus* were studied, and Mn_3O_4NPs showed the highest inhibition diameter(nm) at concentration 100 µg /ml. The inhibitory effect of Mn_3O_4 NPs on the breast cancer cell line (MCF-7) was assessed by determining the half-maximal inhibitory concentration IC_{50}, which was found to be 134.1 µg /ml. This result suggests that the Mn_3O_4 NPs have a strong ability to inhibit cancer cells.

Keywords: *Breast cancer cell line, Green Synthesis, Extract of Spinach plant, nanoparticles.*

التركيب و خصائص مضادات الأغشية الحيوية ومضادات السرطان لجسيمات Mn_3O_4 النانوية المحضرة باستخدام مستخلص نبات السبانخ

نور محمد جاسم , لقاء خالد عبد الكريم *

قسم الكيمياء كلية التربية للعلوم الصرفة ابن الهيثم جامعة بغداد العراق

الخلاصة:

تضمنت هذه الدراسة تخليقًا منخفض التكلفة وصديقًا للبيئة لجسيمات Mn_3O_4 النانوية باستخدام مستخلص السبانخ وكبريتات المنغنيز في وسط قلوي. شخصت جسيمات Mn_3O_4 النانوية باستخدام تقنيات مختلفة، مثل تحويل فوريه للأشعة تحت الحمراء (FTIR)، والأشعة فوق البنفسجية المرئية (UV–visible)، والمجهر الإلكتروني الماسح (SEM) وتقنية حيود الأشعة السينية XRD و تشتت الطاقة بالأشعة السينية EDX وجهد زيتا. حُسب متوسط حجم البلورة عند 46.16 نانومتر باستخدام معادلة ديباي–شيرر، وكان حجم

*Email: likaa.k.a@ihcoedu.uobaghdad.edu.iq

الجسيمات 18.7 نانومتر عند استخدام المجهر الإلكتروني الماسح (SEM)، ولوحظ بعض التشوه نتيجةً للتجمع. أعطى الاستقرار الحركي قيمة ثابتة −52.5 ملي فولت في جهد زيتا لجسيمات Mn_3O_4Nps. دُرست التأثيرات المضادة للبكتيريا لتركيزات (25، 50، و100) ملغم/لتر من جزيئات Mn_3O_4 النانوية ضد بكتيريا المكورات العنقودية الذهبية، والإشريكية القولونية، وفطريات المبيضات، وأظهرت جسيمات Mn_3O_4 النانوية أعلى قطر تثبيط (نانومتر) عند تركيز 100 ملغم/لتر. ودُرست التأثيرات المثبطة لجسيمات Mn_3O_4 النانوية على خلايا سرطان الثدي (MCF−7)، حيث حُسب تثبيط نصف الخلية (IC_{50}) والذي كان مساويًا لـ (134.1 ملغم/مل)، مما يشير إلى قدرة جزيئات Mn_3O_4 النانوية على تثبيط خلايا السرطان.

1. Introduction

Nanotechnology has attracted significant attention across diverse scientific disciplines, including physics, chemistry, biology, engineering, medicine, and materials science, due to its ability to produce complex nanoparticles with tailored size and structure [1,2]. While nanoparticles (NPs) can be synthesized through various approaches, green methods are increasingly preferred in industry due to their lower environmental impact, reduced costs, and viability as alternatives to traditional physical and chemical techniques. In contrast, conventional chemical methods are often expensive and pose environmental and health hazards [3,4]. To achieve a more stable state, the use of chemicals, additives, or both is required. It is not uncommon for synthesis techniques to involve the use of solvents that are neither biodegradable nor polar. Beyond these processes often involve the application of extreme temperatures and pressures [5-7].

Biosynthesis offers an alternative approach to nanoparticle production that does not require the use of hazardous chemicals by utilizing a variety of sources such as bacteria, fungi, algae, and plant extracts. Plant extracts have become a popular choice among these alternative sources due to the stability of the resulting nanoparticles, as well as the relative simplicity, low cost, and lack of environmental damage associated with their synthesis [8-11]. Plant extracts play a crucial role in nanoparticle synthesis by providing preservative and buffering properties. Various plant extracts, such as those from neem (Azadirachta indica), hibiscus (Hibiscus rosa-sinensis), and Indian gooseberry (Emblica officinalis), have been successfully utilized in the synthesis of metal oxide nanoparticles (NPs).

Spinach, in particular, is rich in vitamins A, C, E, and K, as well as folic and oxalic acids, which contribute to its strong antioxidant activity. Additionally, it contains essential minerals such as Mn, Mg, Ca, P, Fe, Zn, Cu, Se, and K. The most significant phytochemicals in spinach include carotenoids (β-carotene, lutein, and zeaxanthin), chlorophyll, glutathione, α-lipoic acid, and betaine, along with various phenolic compounds [12-15]. These plant-derived chemical compounds serve as natural reducing agents in the synthesis of metal oxide nanoparticles. Numerous studies have reported the successful plant-mediated synthesis of MnO_2 nanoparticles using different biological sources, including Euclea natalensis [16] and the pathogenic fungus Fusarium solani [17], plant leave[18] , curcuma longa [19], pomegranate peel [20], cinnamon [21], and others. Research has been conducted on a wide variety of applications, such as adsorption, calculations of thermodynamic functions, the biological effectiveness of Mn_3O_4 NPs, its toxicity, and antioxidants [22], the extract of Thyme plant at pH=12, the Mn_3O_4 NPs was characterized by different techniques, The average crystalline size was calculated using the Debye Scherre equation in value 7.65 nm [23].

The aim of this study was to develop a biocompatible method for synthesizing Mn_3O_4 nanoparticles. Various characterization techniques, including powder metallography, electron

microscopy, atomic force microscopy, and electron density spectroscopy, were employed in some of the nanomaterial diagnostic methods were employed. In addition, as part of the study of its potential applications, its antibacterial properties and the effect of Mn_3O_4 NPs on the MCF-7 cell line were also tested.

2. Methodology

2.1. Materials and Methods

Acquiring specimens, we obtained the spinach from a local source and employed manganese sulfates 98% were bought from Merck Germany, sodium hydroxide 98% from Sigma Aldrich America, and Deionized water from local markets.

The compounds were synthesized and identified using various spectroscopic and microscopic techniques and equipment, including a magnetic stirrer, an electric oven of type PC21-A, Batec, an electric centrifuge of type PLC (80-1), a sensitive electronic balance (AS 220C1) was used for precise measurements. X-ray diffraction (XRD) analysis was performed using a Phillips PW1730 (Netherlands). Ultraviolet-visible spectra are obtained using the Shimadzu UV-160A spectrophotometer. Fourier-transform infrared (FT-IR) spectroscopy was carried out using a Shimadzu 1800 (Japan) within the range of 400-4000 cm^{-1}. The structural and elemental analysis was done using an energy-dispersive X-ray (EDX) spectrometer and a field emission scanning electron microscope (FESEM-EDS) model MIRA II (Czech Republic). Additionally, a transmission electron microscope (TEM) model EM10C-100Kv (Zeiss, Germany) was used for further examination.

2.2. Experiments: Preparation of Spinach Extract and Mn_3O_4 NPs

The same method outlined in [24] was followed. Fresh spinach was collected and thoroughly washed with deionized water to remove any dust or impurities. After drying, it was blended into a fine, uniform powder. Then, 20 grams of this powdered spinach were mixed with 200 mL of deionized water and heated at 70-80°C for 30 minutes while stirring. The mixture was then filtered and stored in the refrigerator for later use. To synthesize manganese oxide nanoparticles using the biosynthesis method, 100 mL of spinach extract was carefully added, drop by drop (one drop per second), to 100 mL of 0.1M $MnSO_4.H_2O$. The solution was stirred for 30 minutes at 70-80°C, and then a sodium hydroxide solution (made by dissolving 2g of NaOH in 50mL of deionized water) was added gradually until the pH reached 12. This method produced a dark green precipitate that underwent purification by repeated washing with deionized water (nearly five times), centrifugation at 4000 rpm for 30 minutes, and decantation. The purified precipitate was then dried in an oven and calcined at 800°C for 3 hours, ultimately producing brown powder from manganese oxide nanoparticles. The Preparation steps of Mn_3O_4 NPs were shown in Figure 1.

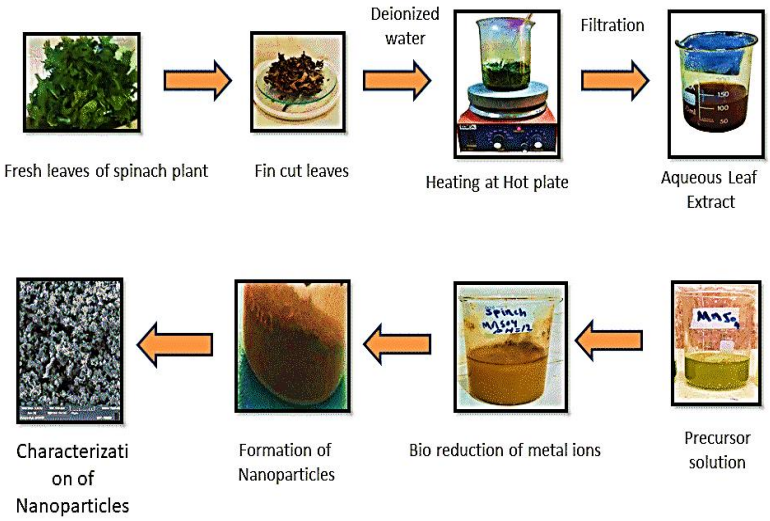

Figure1: Preparation steps of Mn_3O_4 NPs

2.3. Antimicrobials study

Using the disc diffusion technique, the synthesized Mn_3O_4 NPs were examined on Muller Hinton agar, a nutrient medium for bacteria and Potato Dextrose Agar for Candida albicans, to evaluate their antimicrobial activity. The tests were conducted against Staphylococcus aureus (Gram-positive), Escherichia coli (Gram-negative), and the fungal strain Candida albicans. The petri dishes were incubated at 37°C for bacteria and 25–30°C for fungi for 24 hours, after which the diameter of the inhibition zone, indicating bacterial growth suppression, was measured. To assess the bactericidal properties of the synthesized Mn_3O_4 nanoparticles, standard antibiotics were used for comparison. The Mn_3O_4 NPs concentrations tested were 25%, 50%, and 100% µg /ml, prepared in a DMSO solvent as a control [22].

2.4. Cytotoxic Assays

The MTT assay was employed to evaluate the activity of Mn_3O_4 NPs at various concentrations (25, 50, 100, 200, and 400) µg/mL against MCF-7 breast cancer cell lines. This colorimetric technique was used to assess the metabolic activity of the cells and determine the extent to which the nanoparticles affected cancer cell viability [23].

2.5. Antibiofilm Assays

The ability of our compound to inhibit biofilm formation was evaluated following the protocol described in [24]. First, 100 µL of brain heart infusion (BHI) broth containing *Staphylococcus aureus* was inoculated into a sterile, flat-bottomed 96-well microtiter plate (MTP). Then, 100 µL of the test compound was added to each well, and the plate was incubated at 37°C for 24 hours without shaking. After incubation, the wells were carefully emptied and washed three times with sterile phosphate-buffered saline (PBS) to remove unattached (planktonic) bacteria. The plates were then dried in an oven at 60°C for 45 minutes. Following this, 150 µL of a 1% crystal violet solution was added to each well and incubated at room temperature for 20 minutes. Excess stain was removed by washing the wells at least three times with PBS. Finally, the crystal violet bound to the adherent biofilm was dissolved using 150 µL of 95% ethanol to destain the wells.

2.6. Biofilm Inhibition percentage % calculation

The absorbance of the plates was measured at 590 nm using an ELISA microplate reader. The average absorbance (OD) of each sample was calculated, and the results were expressed as a percentage of biofilm inhibition using the following equation [24]:

Percentage of cell viability $\frac{(OD\ value\ in\ the\ experiment\ group - OD\ value\ in\ the\ blank\ well)}{(OD\ value\ in\ the\ control\ group - OD\ value\ in\ the\ blank\ well)} \times 100\%$

3. Results and Discussion

3.1. FT-IR analysis

FTIR spectrum of Mn_3O_4 NPs, recorded over the range (4000-400) cm^{-1} and shown in figure 2, exhibits bands at 524 cm^{-1}, 617cm^{-1} and 989 cm^{-1} attributed to Mn-O vibrations [23,24]. The bands at (3390, 1633 and 1469) cm^{-1} were due to remaining active groups in the plant extract might be the cause of the other bands' vibration stretching of O-H, C=C and C=O, respectively, and the 3016 cm^{-1} band suggests C–H stretching from aliphatic groups [25].

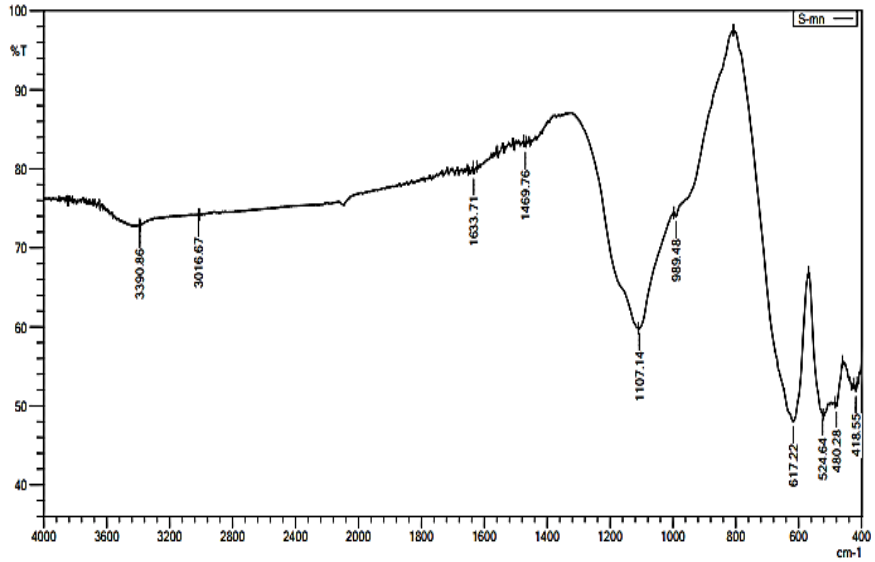

Figure 2: FT-IR spectrum for Mn_3O_4 NPs

3.2. UV-Visible analysis

Mn_3O_4 nanostructures exhibit unique optical properties in the UV-visible region, including characteristic absorption peaks. These peaks are attributed to charge transfer transitions, particularly those involving the O^{2-} to Mn^{2+} and O^{2-} to Mn^{3+} transitions. The UV-vis spectrum of Mn_3O_4 NPs in 10^{-3}M concentration and DMSO as a solvent typically shows absorption peaks around 291 nm and 350 nm, indicating the formation of the nanoparticles. Additionally, the UV-vis spectrum can be used to analyze the optical bandgap of Mn_3O_4 NPs, which is influenced by factors like the presence of other materials or the size of the nanoparticles.

The band gap value can be determined from the fundamental absorption, which corresponds to electron excitation from the valence band to the conduction band. The absorption coefficient (α) and the incident photon energy (hν) are related to the Tauc's formula [26] given by the equation:

$(\alpha h\nu)n = K(h\nu - Eg)$.

Where hν is the photon energy, α is the absorption coefficient, K is a constant, Eg is the bandgap energy, and the value of n is 2 for direct allowed transitions, while it is ½ for indirect allowed transitions.

The variation of (αhν) 2 vs. hν for the Mn_3O_4 NPs (Fig. 4) shows that the extrapolation of the linear portion to the hν axis gives the energy gap of the direct bandgap .
The value of band gap energy of Mn_3O_4 NPs with an average crystalline size was calculated by assuming the direct transition i.e., n=2, because the optical absorption in Mn3O4 is direct allowed.

The direct bandgap values for the Mn_3O_4 nanoparticles were observed to be 4.26 and 3,54 eV, which is quite larger than the conventional [26].

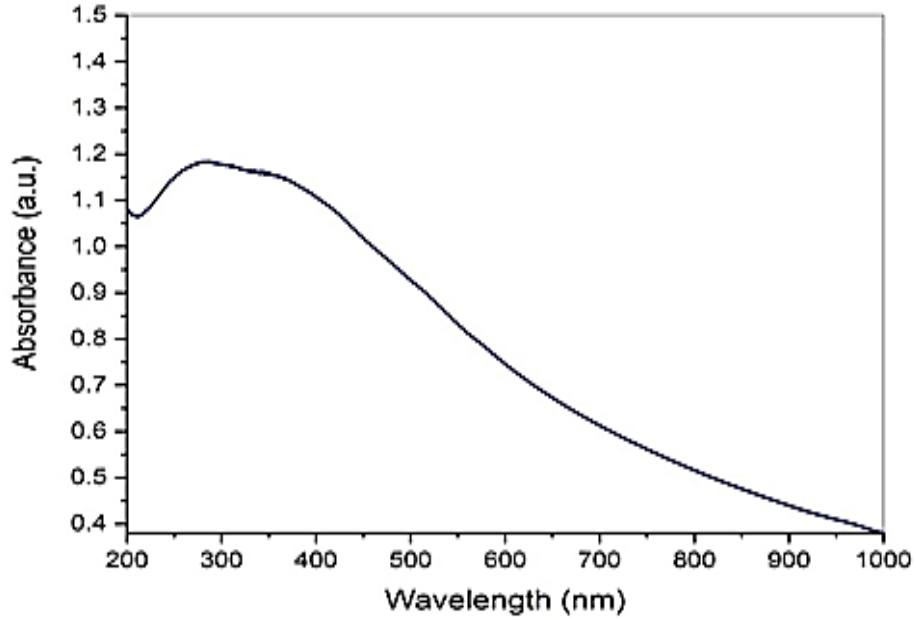

Figure 3: UV visible spectrum of Mn_3O_4 NPs

3.3. The XRD and EDX Analyses

Based on the X-ray diffraction (XRD) study shown in Table 1 and Figure 4, it has been determined that the crystal planes of Mn_3O_4 NPs, the crystal planes of Mn_3O_4 NPs were identified and matched with Miller indices 101, 103, 202, 321 and 224. These correspond to diffraction peaks observed at 2θ values of 29.221°, 32.704°, 36.397°, 58.760°, and 60.175°, respectively. The average crystalline size (**D**) was determined using the Scherrer equation, ($D = 0.9 \lambda / \beta \cos \theta$) where D= The average crystalline size, the Cu K X-ray radiation (λ = 1.5418 ºA), was discovered to be approximately 46.160 nm. The angles observed in the diffraction pattern of Mn_3O_4 NPs closely match the conventional diffraction peaks of JCPDS card number (00-008-0017) [26].

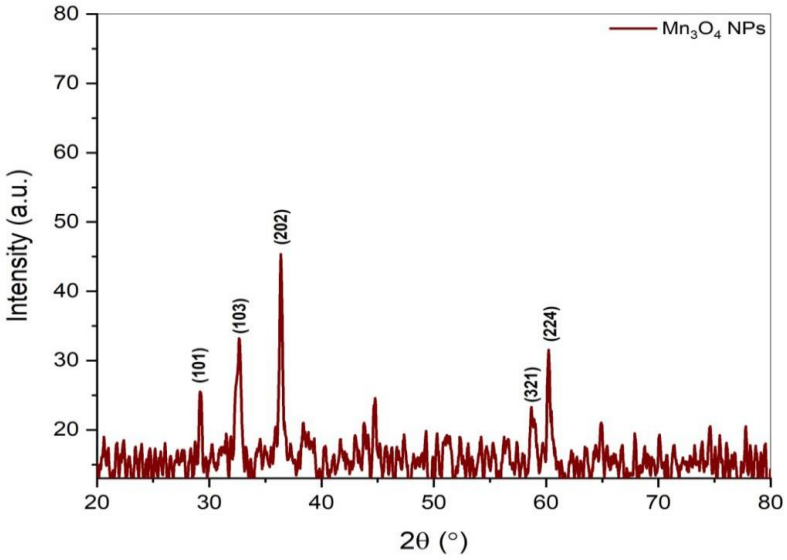

Figure 4: The XRD pattern of Mn_3O_4 NPs

Table 1: The XRD details for Mn_3O_4 NPs.

Pos. [°2Th.]	hkl	FWHM (deg)	2 theta (Rad.)	FWHM (Rad.)	crystal size (nm)	Average crystal size (nm)
29.221	101	0.1358	0.255001	0.002	60.435	
32.704	103	0.1811	0.285396	0.003	45.709	
36.397	202	0.2263	0.317627	0.004	36.936	46.16
58.760	321	0.4526	0.512779	0.008	20.134	
60.175	224	0.1358	0.525129	0.002	67.587	

EDX was used to analyze the percentage of elements in the sample, and the results obtained from this analysis revealed a characteristic peak associated with the % element composition (Mn and O), which corresponds to the exact composition of the sample under study, as shown in Figure 5. The element percentages showed 80% for manganese and 20% for oxygen [26].

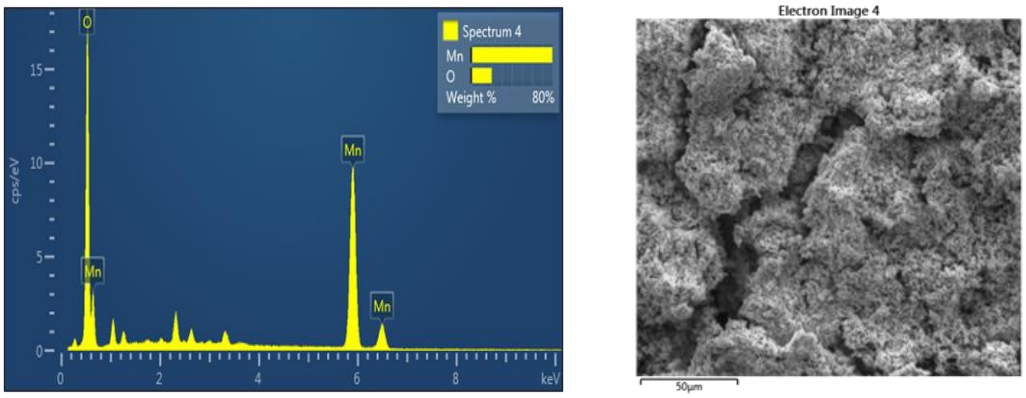

Figure 5: The EDX of Mn_3O_4 NPs

3.4. SEM and TEM analyses

SEM analysis revealed Mn_3O_4 NPs with nanostructured morphology (Figure 5), showing spherical particles with an average diameter of 18.7 nm.

TEM analysis (Figure 6) confirmed spherical morphology with narrow size distribution. Images were acquired at 20 kV accelerating voltage (SEM) and 200 kV (TEM), Size distribution analysis of 100 particles showed 90% within the (15-22) nm range. The spherical morphology (confirmed by TEM) enhances surface-area-to-volume ratio, which is beneficial for catalytic applications [27]. Uniform particle size distribution suggests controlled nucleation/growth during green synthesis

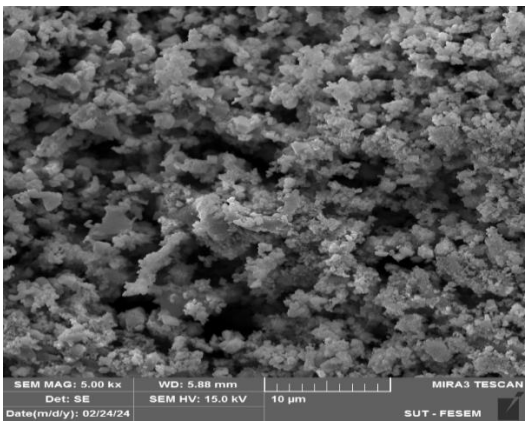

Figure 6: The images of SME for Mn_3O_4NPs

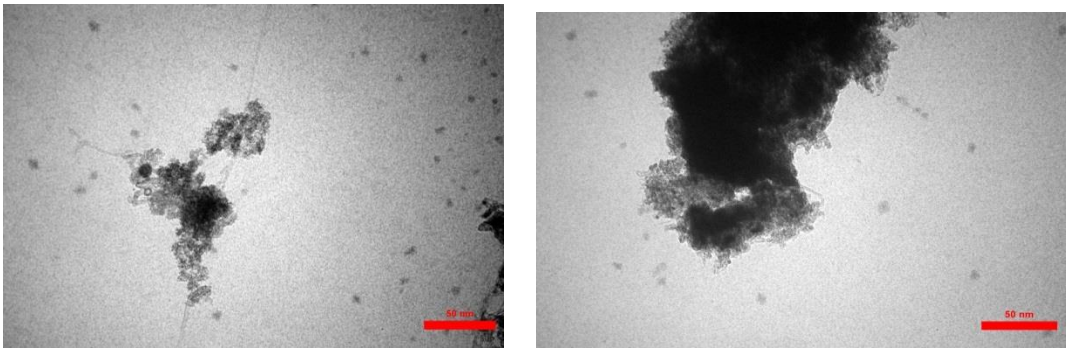

Figure7: TEM images of Mn_3O_4 NPs

3.5. Zeta potential of Mn_3O_4Nps

The zeta potential of the Mn_3O_4 NPs synthesized using spinach plant extract was measured at -52.5 mV, as illustrated in Figure 8. This showed that the kinetic stability of the Mn_3O_4Nps system would persist for a long time and at high surface charge, and thus can remain in suspended form in solution [28].

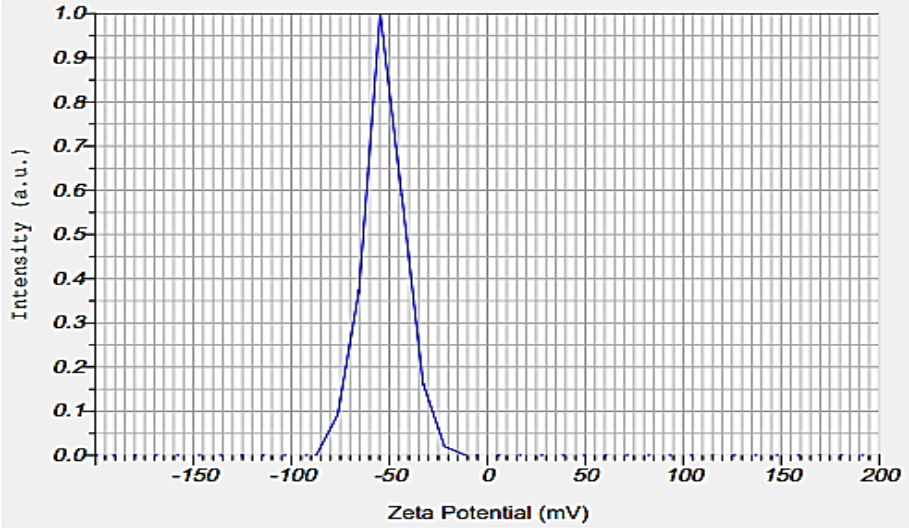

Figure 8: The images of the Zeta potential of Mn_3O_4Nps

3.6. Antimicrobials Activity

The antibacterial activity of the Mn_3O_4 NPs synthesized from spinach plant extract was assessed using the agar well diffusion method [29]. The nanoparticles were tested at concentrations of 25 µg /ml, 50 µg /ml, and 100 µg /ml in a DMSO as a solvent to evaluate their effectiveness against bacterial strains. The results of this evaluation are depicted in Figure 9 and Table 2. *Staphylococcus aureus, E.coil*, and *Candida fungus* were the organisms that were investigated. The antibiotics were tested on these bacteria and fungi, which served as controls. The antimicrobial effect of Mn_3O_4 NPs was evaluated by analyzing the growth inhibition zone against the used pathogens. This occurred after varying the concentration of the nanoparticles several times. According to the results, good inhibition against different bacterial species was achieved at all three concentrations, but at 25% concentration, inhibition against fungi was lower compared to the other concentrations. It was found that the antimicrobial effect of metal nanoparticles against bacteria depended on the concentration of metal nanoparticles and was closely associated with the formation of pits in the bacterial cell wall, which impaired the ability of the bacteria to continuously form the cell wall, leading to the disintegration of the bacterial cell wall. Several key factors influence the antibacterial activity of metal oxides, including the nature of the metal ion, its coordinating site, and hydrophobicity [30, 31].

Table 2: The Zone Inhibition in (mm) of Mn_3O_4NPs against Different Microbial

Conc. µg /mL	*Escherichia coli*	*Staphylococcus aureus*	*Candida albicans*
25	11	11	5
50	12	12	4
100	14	13	10

Figure 9: The Antibacterial activity of Mn_3O_4 NPs from Spinach plant extract

3.7. Anticancer Assay Study

The inhibitory activity of Mn_3O_4 NPs against MCF-7 cell proliferation was tested at doses of 25, 50, 100, 200, and 400 µg/mL, with doxorubicin serving as the positive control [33,23]. Increasing the concentrations of Mn_3O_4 NPs and doxorubicin resulted in reduced cell viability, as shown in Table 3 and Figure 10. Mn_3O_4 NPs, when tested against MCF-7 at a concentration of 400 µg /ml, showed a viability was 71.489. It is the concentration value when the inhibition is at the value, as seen in Figure 11. The lower IC_{50} value of 134.1 µg /ml is shown in Figure 12.

Table 3: Viability (%) of Mn_3O_4 NPs and Standard Drug against MCF-7 Cell Lines

Conc. µg/mL	HdFn		MCF-7	
	mean	SD	Mean	SD
400	71.48933	3.918762	52.585	4.180124
200	86.034	0.853534	63.696	2.122644
100	92.12967	1.557424	77.62333	2.411951
50	96.18033	1.251681	90.58667	1.801743
25	96.95233	1.141793	94.79167	1.334742

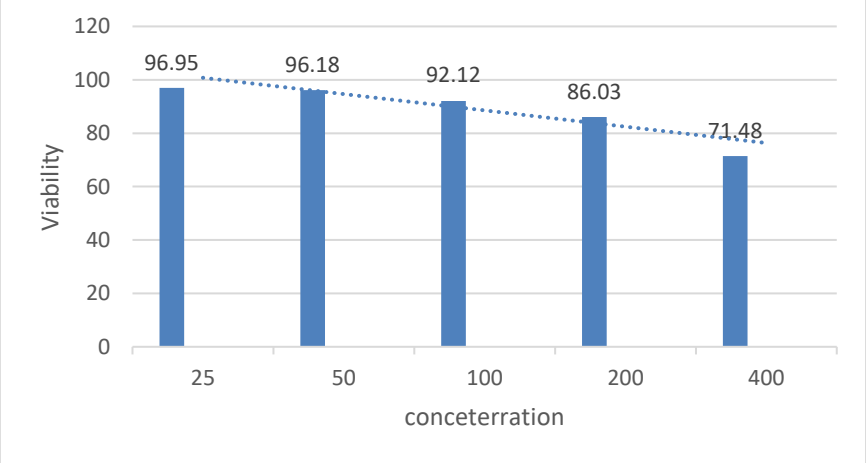

Figure 10: The viability for Mn_3O_4 NPs against HdFn cell lines

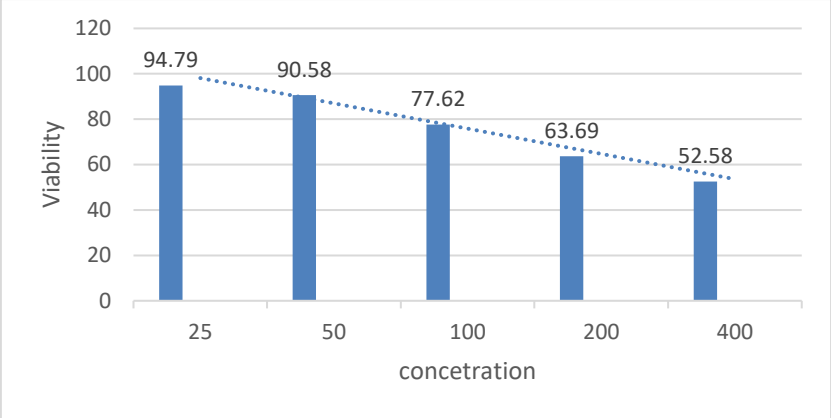

Figure 11: The viability for Mn_3O_4 NPs against MCF-7 cell lines

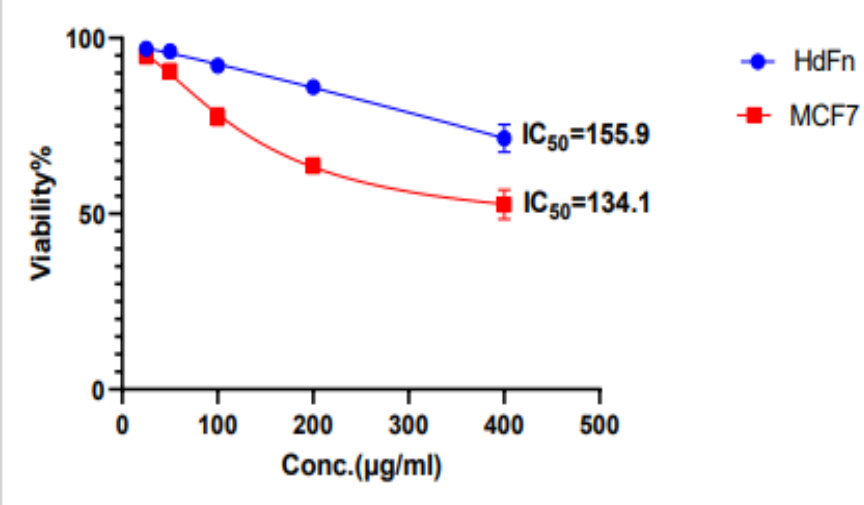

Figure 12: The Mn_3O_4 NPs of IC_{50} (134.1 µg/mL)

3.8. Antibiofilm assessment analysis

OD590 measurements were performed in triplicate after 10 min CV staining and ethanol solubilization.

The antibiofilm inhibition percentage ABF% was calculated as $[1- (OD_{treated}/OD_{control})]\times100$. Mn_3O_4 NPs (100 µg/mL) showed 98% inhibition against *S. aureus* (Gram+) and 97% against *E. coli (Gram-)* biofilms. Despite structural differences, similar inhibition suggests disruption of conserved biofilm components like extracellular DNA or polysaccharides. Three technical replicates showed <5% variation between measurements. Figure 13 demonstrates complete biofilm eradication in treated wells versus dense control biofilms [34,35].

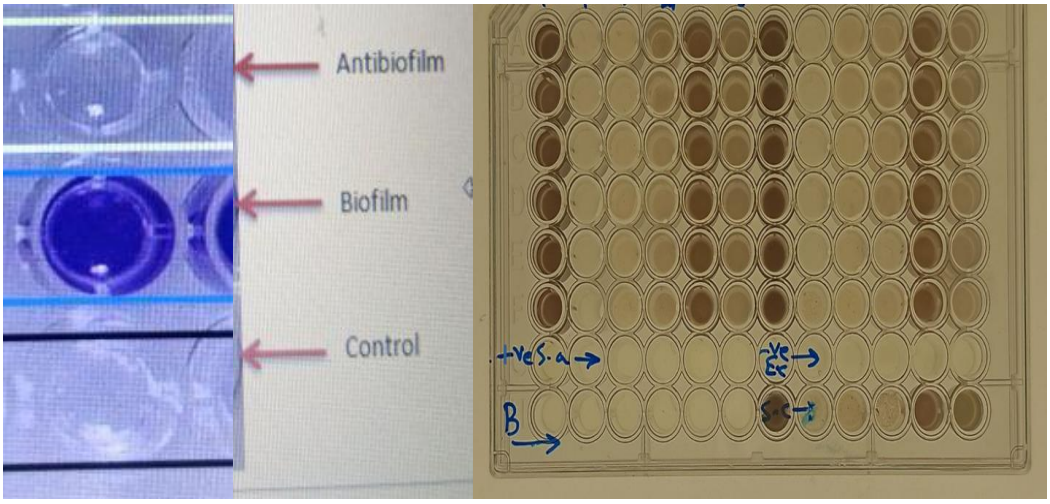

Figure 13: a) The effect of biofilm and Antibiofilm of Mn_3O_4 NPs b) The mtp filled with broth media + materials before incubation; Column from 1A to 6 F processed for Gram+ve bacteria; Column from 7A to 12 F processed for Gram –ve bacteria. B –Blank (media control); S.c- Sample control of Mn_3O_4 NPs

Conclusion

This study presents an efficient and environmentally friendly method for synthesizing Mn_3O_4 NPs using Spinach plant extracts. The synthesized Mn_3O_4 NPs were thoroughly characterized by FTIR and UV-Visible, Zeta potential, SEM, EDX and XRD techniques to assess their surface morphology and composition. SEM analysis revealed 18.7 nm, the size of average crystal size was 46.16 nm in XRD, the particles are small and spherical due to aggregation, and EDX showed Mn:O ratio of 4:1, matching Mn_3O_4 stoichiometry, which contained 80% manganese and 20% oxygen. The antibiofilm inhibition percentage of the tested material was determined to be 98% against Gram-positive bacteria and 97% against Gram-negative bacteria. The efficacy of Mn_3O_4 NPs against various antimicrobials was found to be the zone inhibition diameters of 12±2 mm (S. aureus) vs 12±1 mm (E. coli). Mn_3O_4 NPs have anticancer action against MCF7 with a value of (134.1) µg/mL for IC_{50}.

Acknowledgment:

The authors would like to express their sincere gratitude to the Chemistry Department of Ibn-Al Haitham University in Baghdad, Iraq, for their generous financial support of this research.

Disclosure Statement: *Conflict of Interest: The authors declare no conflicts of interest. Compliance with Ethical Standards: This article does not involve any studies conducted on human or animal subjects.*

Reference

[1] A. Karnwal, A. Y. Jassim, A. A. Mohammed, V. Sharma, A. R. M. S. Al-Tawaha and I. Sivanesan, "Nanotechnology for Healthcare: Plant-Derived Nanoparticles in Disease Treatment and Regenerative Medicine," *Pharmaceuticals*, vol. 17, no. 12, p. 1711, 2024. doi: 10.3390/ph17121711.

[2] S. J. Eichhorn et al., "Current international research into cellulose as a functional nanomaterial for advanced applications," *Journal of Materials Science*, vol. 57, no. 10, pp. 5697–5767, 2022. doi: 10.1007/s10853-022-06903-8.

[3] A. A. Hafez, P. Naserzadeh, K. Ashtari, A. M. Mortazavian and A. Salimi, "Protection of manganese oxide nanoparticles-induced liver and kidney damage by vitamin D," *Regulatory Toxicology and Pharmacology*, vol. 98, pp. 240–244, 2018.

[4] M. A. Abduljabar and S. H. Merza, "Graphene Oxide Decorated with Nickel Cobaltite Nanoparticles as an Adsorbent for Cationic Methyl Green Dye: Kinetic, Isotherm, and Thermodynamic Studies," *Baghdad Science Journal*, 2024.

[5] K. S. Ahmad, S. Yaqoob and M. M. Gul, "Dynamic green synthesis of iron oxide and manganese oxide nanoparticles and their cogent antimicrobial, environmental and electrical applications," *Reviews in Inorganic Chemistry*, vol. 42, no. 3, pp. 239–263, 2022.

[6] M. Perachiselvi, M. S. Bagavathy, J. J. Samraj, E. Pushpalaksmi and G. Annadurai, "Synthesis and characterization of Mn3O4 nanoparticles for biological studies," *Applied Ecology and Environmental Sciences*, vol. 8, no. 5, pp. 273–277, 2020.

[7] M. Fang et al., "Low-temperature synthesis of Mn3O4 hollow-tetrakaidecahedrons and their application in electrochemical capacitors," *CrystEngComm*, vol. 13, no. 15, pp. 4915–4920, 2011.

[8] C. Fernandes et al., "Photodamage and photoprotection: toward safety and sustainability through nanotechnology solutions," *Food Preservation, Academic Press*, 2017, pp. 527–565.

[9] L. J. Frewer et al., "Consumer attitudes towards nanotechnologies applied to food production," *Trends in Food Science & Technology*, vol. 40, no. 2, pp. 211–225, 2014.

[10] A. Nande et al., "Green synthesis of nanomaterials using plant extract: a review," *Current Pharmaceutical Biotechnology*, vol. 22, no. 13, pp. 1794–1811, 2021.

[11] A. Sukhdev et al., "Synthesis, phase transformation, and morphology of hausmannite Mn3O4 nanoparticles: photocatalytic and antibacterial investigations," *Heliyon*, vol. 6, no. 1, 2020.

[12] Z. E. Jiménez-Pérez et al., "Applications of Panax ginseng leaves-mediated gold nanoparticles in cosmetics relation to antioxidant, moisture retention, and whitening effect on B16BL6 cells," *Journal of Ginseng Research*, vol. 42, no. 3, pp. 327–333, 2018.

[13] S. Khan et al., "In vitro evaluation of anticancer and biological activities of synthesized manganese oxide nanoparticles," *MedChemComm*, vol. 7, no. 8, pp. 1647–1653, 2016.

[14] A. Vijayakumar, A. Chacko and P. Jayaprakash, "Green synthesis of Mn3O4 nanoparticles in zinc chloride: Urea: acetamide deep eutectic solvent-characterization, fluorescence sensing, antibacterial and antioxidant properties," *Journal of Molecular Structure*, vol. 1321, p. 139833, 2025.

[15] J. Sackey et al., "Molecular dynamics and bio-synthesis of phoenix dactylifera mediated Mn3O4 nanoparticles: Electrochemical application," *Journal of Alloys and Compounds*, vol. 854, p. 156987, 2021.

[16] M. R. Shaik et al., "Mn3O4 nanoparticles: Synthesis, characterization and their antimicrobial and anticancer activity against A549 and MCF-7 cell lines," *Saudi Journal of Biological Sciences*, vol. 28, no. 2, pp. 1196–1202, 2021.

[17] T. Van Tran et al., "Green synthesis of Mn3O4 nanoparticles using Costus woodsonii flowers extract for effective removal of malachite green dye," *Environmental Research*, vol. 214, p. 113925, 2022.

[18] Y. Wang et al., "Dye degradation studies of hausmannite manganese oxide (Mn3O4) nanoparticles synthesized by chemical method," *Applied Physics A*, vol. 127, no. 4, p. 277, 2021.

[19] A. H. Majeed et al., "A review on polyaniline: synthesis, properties, nanocomposites, and electrochemical applications," *International Journal of Polymer Science*, vol. 2022, p. 9047554, 2022. doi: 10.1155/2022/9047554.

[20] N. J. Mohammed and L. K. Abdul Karem, " Biosynthesis, Characterization, Antibiofilm and Anticancer Assay of Zirconium Oxide Nanoparticles using Spinach Plant Extract," *Moroccan Journal of Chemistry*, vol. 14, no. 3, pp. 884-897, 2026. doi: 10.48317/IMIST.PRSM/morjchem-v14i3.51039.

[21] A. H. Ali, Z. H. Shakir, A. N. Mazher and S. N. Mazhir, "Influence of Cold Plasma on Sesame Paste and the Nano Sesame Paste Based on Co-occurrence Matrix," *Baghdad Science Journal*, vol. 19, no. 4, p. 0855, 2022. doi: 10.21123/bsj.2022.19.4.0855.

[22] R. S. Sahib and J. A. Naser, "Preparation, characterization and surface area properties of manganese oxide nanoparticles," *Annals of the Romanian Society for Cell Biology*, vol. 25, no. 5, pp. 2962–2969, 2021.

[23] S.H. El-Moslamy , Y.A. El-Maradny, M.H. El-Sayed, M.A. El-Sakhawy, and E.M. El-Fakharany,“ Facile phyto-mediated synthesis of ternary CuO/Mn3O4/ZnO nanocomposite using

Nigella sativa seeds extract: characterization, antimicrobial, and biomedical evaluations", Scientific Reports, vol. 15, no. 1, pp. 16139, 2025, doi: 10.1038/s41598-024-85044-1.

[24] R. A. Hussein, F. W. Abdul Aziz, H. H. Al-Haideri and S. A. Al-Qaysi, "Novel biosynthesis of manganese dioxide nanoparticles using watermelon peel extract and their biological applications," *Microbial Biosystems*, vol. 10, no. 1, pp. 112–122, 2025. doi: 10.21608/mb.2025.314779.1155.

[25] D. N. Binjawhar, N. M. Al-Enazi, K. Alsamhary and M. Kha, "Plant mediated biosynthesis of Mn3O4 nanostructures and their biomedical applications," *Heliyon*, vol. 10, no. 6, 2024.

[26] H. H. Farhan and A. M. Mohammed, "Biosynthesis and evaluation of MnO2 nanoparticles as anti-oxidant and anti-diabetic agents," *Results in Chemistry*, vol. 7, p. 101266, 2024.

[27] Z. R. Al Bahadili, A. A. S. Al Hamdani, L. A. Al Zubaidi, F. A. Rashid and S. M. Ibrahim, "An evaluation of the activity of prepared zinc nano-particles with extract alfalfa plant in the treatments of peptidase and ions in water," *Baghdad Science Journal*, vol. 6, no. 7, pp. 522–533, 2022.

[28] P. Chaudhary, C. Kumari, A. Singh, M. Vijay, A.K. Jangir, S. Jadoun, and N.K. Jangid, " Transforming Citrus sinensis Seed Waste Into Modified MnO2 Nanoparticles as Photocatalytic and Biological Agent", *Chemistry Select*, vol. 11, no. 9, pp. e03865, 2026, doi: 10.24996/ijs.2024.65.11.4.

[29] M. D. Ruaa, S. A. Alsahib and I. F. Ascar, "Synthesis, characterization and cyclazation of pyran using Ag2O nanoparticle from natural source "ginger"," *Iraqi Journal of Agricultural Sciences*, vol. 52, no. 5, pp. 1171–1184, 2021. doi: 10.36103/ijas.v52i5.1455.

[30] R.H. Salman, and L.K.A. Karem, " Degradation Of Methylene Blue Dye Using Biologically Synthesized of Mn3O4: Ag Nanocomposites by Thyme Leaves Extract", *Macromolecular Symposia*, vol. 415, no. 1, pp. e70162, February. 2026, doi: 10.1002/masy.70162.

[31] T. M. Al-Saadi, "Investigating the Structural and Magnetic Properties of Nickel Oxide Nanoparticles Prepared by Precipitation Method," *Ibn Al-Haitham Journal for Pure and Applied Sciences*, vol. 35, no. 4, pp. 94–103, 2022. doi: 10.30526/35.4.2872.

[32] A. A. Majeed and A. M. N. Khaleel, "Evaluation of the anticancer and biological activity of a new amide compound of trimethoprim with some of its complexes," *Caspian Journal of Environmental Sciences*, vol. 22, no. 1, pp. 9–22, 2024, DOI: 10.22124/cjes.2023.7323 .

[33] S.A. Mousa, H. Abdallah and S.A. Khairy, " The use of green synthesized TiO2/MnO2 nanoparticles in solar power membranes for pulp and paper industry wastewater treatment", *Scientific Reports*, vol. 15, no. 1, pp. 4281–4290, Jun. 2025, doi: 10.1038/s41598-024-85075-8.

[34] A.B. Dileepan, and S. Jeyaram , " Sustainable industrial wastewater via photocatalysis using green-synthesised MnO2 nanoparticles," *Materials Research Innovations*, Vol.30, no.1, pp. 62-87, Jun. 2025, doi: 10.1080/14328917.2025.2534542.